

Flexible Blade-Coated Optoelectronic Devices: Dual Functionality via Simultaneous Deposition

Jasmine Jan, Juan Zhu, Jonathan Ting, and Ana C. Arias*

Advances in printing techniques have enabled a new generation of low-cost and large-area flexible electronics. However, in applications where a combination of printed components is required, multiple fabrication processes and subsequent integration can be complex and time consuming. Additionally, these applications require devices to be stacked atop each other, reducing overall mechanical flexibility. In this work, surface-energy-patterning (SEP) is used to enable simultaneous blade coating of organic photodiode (OPD) and organic light-emitting diode (OLED) films side-by-side. The result is dual functionality on a single flexible substrate. Various active layer solution concentrations are investigated to optimize active layer thicknesses and consequently optimize the performance of each device. A peak spectral responsivity of 0.33 A W^{-1} at 800 nm is achieved for optimized OPDs and a maximum luminance of 7000 cd m^{-2} is achieved for optimized OLEDs at an applied bias of 8 V . Overall, this technique enables the printing of two functionally distinct devices in a single step without compromising the performance of either device.

urements.^[8,9] Fabrication of such a dual device system requires a series of separate time-consuming printing steps optimized for each device. In reflectance mode oximetry, where the optoelectronics are on the same plane, laminating substrates reduces the mechanical flexibility of the overall system.^[10] Configuring connections between devices on separate substrates to external circuitry can also add complexity to the integration. Overall, there is a need to reduce process complexity and fabrication time of multifunctional systems.

Blade coating is a printing method that has been used for fabrication of organic devices including thin-film transistors,^[11,12] light-emitting diodes,^[13–15] photodiodes,^[16,17] and photovoltaics.^[18] With this method, large-area films can be tuned to the desired film thickness through optimization in coating speed, blade height, processing

temperature, and solution properties.^[19,20] Traditionally, a blade coating process is designed for depositing one film at a time, limiting its use to single-function systems. We have recently shown a method to blade-coat two light-emitting diodes in a single printing step.^[13] To advance this work, we demonstrate the simultaneous deposition of an organic photodiode (OPD) and organic light-emitting diode (OLED) side-by-side on a single flexible substrate. Whereas there may be tolerance for two OLED solutions to intermix during blade coating without significantly affecting the final emission of either OLED, OPD and OLED materials are functionally distinct and require more controlled separation of the deposited solutions. The surface of the substrate is treated and patterned to isolate the two solutions during blade coating. Additionally, OPD and OLED devices require different active layer film thicknesses for optimal device performance. We tuned solution concentrations to achieve the desired film thicknesses and optimize device characteristics. Overall, we demonstrate the deposition of multifunctional devices on a single substrate. This method accelerates fabrication time, retains flexibility of a single substrate system, and decreases integration complexity for flexible electronic applications.

1. Introduction

In recent years, there has been a rise of flexible electronics in wearables,^[1] healthcare,^[2] and consumer electronics.^[3] The shift away from rigid electronics is driven by the desire for form factors that are soft and conforming, facilitating improved interfacing with the body and other dynamic surfaces.^[4,5] Developments in flexible electronics have also enabled properties that cannot be satisfied with conventional electronics such as folding, rolling, and stretching.^[6,7] Printing has emerged as a promising and commercially viable method for high-throughput fabrication of low-cost flexible electronic systems. Whereas traditional silicon IC microfabrication relies on a series of subtractive steps for patterning structures, printing utilizes a series of additive steps that are scalable to high-throughput roll-to-roll manufacturing.

In many flexible electronic applications, integration of multiple devices is necessary. For example, a combination of light-emitting diodes (LEDs) and photodiodes (PDs) is necessary for photoplethysmogram (PPG) and pulse oxygenation meas-

J. Jan, J. Zhu, J. Ting, A. C. Arias
Department of Electrical Engineering and Computer Sciences
University of California
Berkeley, CA 94720, USA
E-mail: acarias@berkeley.edu

 The ORCID identification number(s) for the author(s) of this article can be found under <https://doi.org/10.1002/adfm.202112343>.

DOI: 10.1002/adfm.202112343

2. Results and Discussion

2.1. Printing Process

The illustration of the simultaneous printing process is shown in **Figure 1**. A self-assembled monolayer (SAM) of hydrophobic

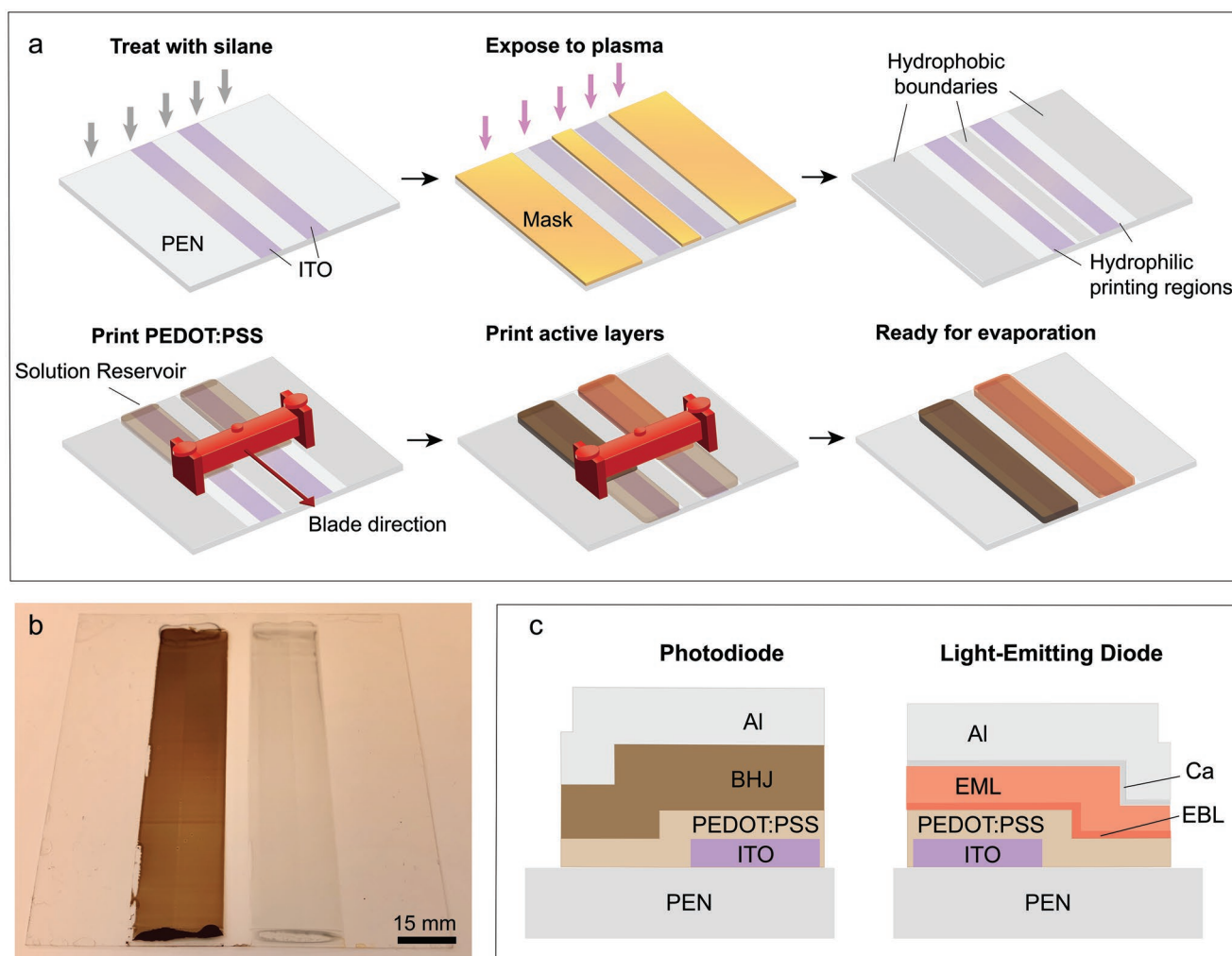


Figure 1. a) Illustration of surface energy patterning and simultaneous printing process. The ITO/PEN patterned substrate is treated with a blanket vapor deposition of hydrophobic silane. A polyimide tape is applied in designated regions and the substrate is exposed to plasma, resulting in two hydrophilic printing regions surrounded by hydrophobic boundaries on the surface of the flexible substrate. PEDOT:PSS and active layers are all printed via blade coating. b) Image of dried films after printing and prior to evaporation. c) Illustration of complete film stacks for the OPD and OLED.

silane is vapor deposited on a polyethylene naphthalate (PEN) substrate patterned with indium-tin-oxide (ITO) as working anodes. Polyimide tape is applied as a protection mask for SAMs in designated regions, and the substrate is exposed to low-energy plasma. The result after removing the polyimide tape is a substrate surface with two hydrophilic printing regions surrounded by hydrophobic boundaries. Organic layers for both devices are then deposited via blade coating. Poly(3,4-ethylenedioxythiophene) doped with poly(styrenesulfonate) (PEDOT:PSS) is deposited via blade coating followed by blade coating of the bulk heterojunction (BHJ) for the OPD and electron blocking layer (EBL) and emissive layer (EML) for the OLED. Working cathodes are then thermally evaporated onto printed organic layers. Figure 1b shows an image of dried films after printing steps are completed and Figure 1c shows the full device stack fabricated in this work.

Isolation of the OPD and OLED solutions is crucial as inadvertent contact between the two semiconducting materials results in a loss of device functionalities. OPD BHJ materials

are optimized for efficient absorption of photons and dissociation of excitons in response to light whereas OLED EML materials are optimized for generation and recombination of excitons in response to injected current. These opposing optoelectronic mechanisms interfere when the two materials are mixed, negatively affecting device performances.

During printing, separation of solutions along both the substrate and the blade is necessary as the materials are still wet and have the mobility to coalesce. Contact angle measurements were used to analyze the wettability of solutions on each surface in this process. Figure 2 shows contact angles of water (a–c), OLED EML solution (d–f), and OPD BHJ solution (g–i) on the printing surface (green), the silane surface (orange), and the doctor blade surface (blue). Water spreads on the surface of the plasma-treated substrate (contact angle $<5^\circ$) and dewets on the hydrophobic silane (110°). Furthermore, water is hydrophobic on the surface of the doctor blade, exhibiting incomplete wetting (90°). As a result of the high contrast in wetting behavior between the

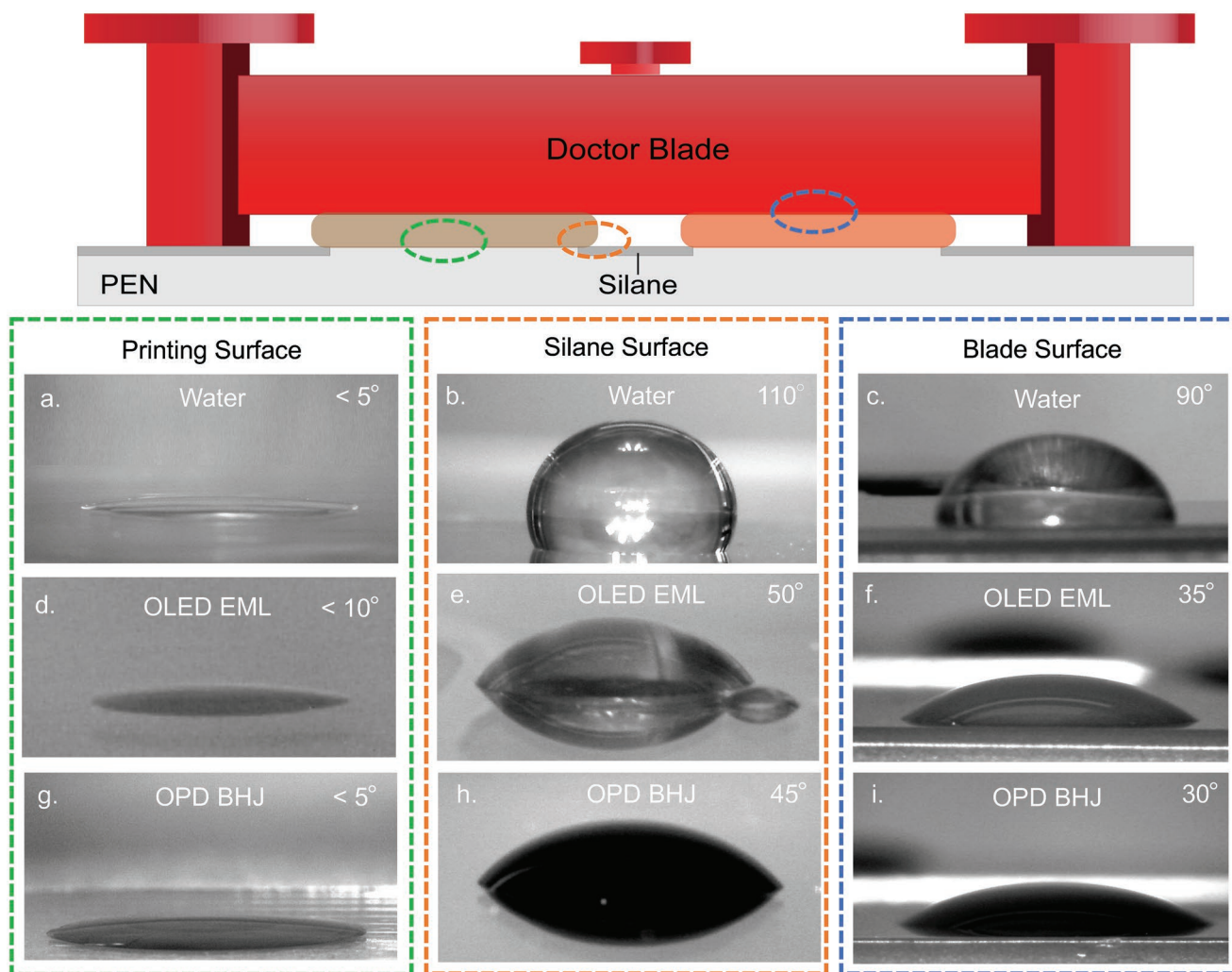


Figure 2. The contact angles of solutions on three surfaces are used in this process. The three solutions are water, the OLED EML solution, and the OPD BHJ solution. (a, d, g in the green box) All three solutions exhibit near-complete wetting on their respective printing surface. The respective printing surfaces are a) plasma-treated substrate, d) dried EBL film and g) dried PEDOT:PSS. (b, e, h in the orange box) The solution–silane interface shows water has the highest contact angle with OLED and OPD showing similar partial wetting behavior on the surface of silane. (c, f, i in the blue box) The solution–blade interface shows that water spreads the least on blade surface, while both organic solutions exhibit good wetting on the blade surface.

printing region and the other two surfaces, no merging of PEDOT:PSS, a water-based solution, was observed. On the other hand, the contact angle disparity for the organic solutions is smaller. Organic solutions show near-complete wetting on their respective printing surfaces with OLED EML exhibiting $<10^\circ$ on dried EBL film and OPD BHJ exhibiting $<5^\circ$ on dried PEDOT:PSS film. On the silane surface, organic solutions exhibit partial wetting (50° and 45°). However, on the blade surface, organic solutions achieve good wetting (35° and 30°). Thus, the organic solutions were observed to spread along the blade and coalesce during printing when there is an excess of solution. This can be seen in Figure S1 (Supporting Information) where the OPD BHJ solution merged with the OLED EML solution via travel across the blade. To mitigate this issue, deposited solution volume was optimized to decrease spreading and avoid solution merging.

2.2. Device Performance Optimization

Organic materials are optimized to achieve high device performance.^[21,22] Based on desired device characteristics, the blade coating parameters are optimized for the thickness of the resulting film. The printed film thickness t is related to blade coating parameters in the following:

$$t_{\text{wet film}} \propto \left(\frac{\mu V_{\text{blade}}}{\gamma} \right)^{2/3} (R_{\text{meniscus}}) \quad (1)$$

where μ is the solution viscosity, V_{blade} is the coating speed, γ is the solution surface tension, and R_{meniscus} is the radius of curvature of the solution trailing the moving blade.^[19] Contrary to spin coating where film thickness is inversely related to the

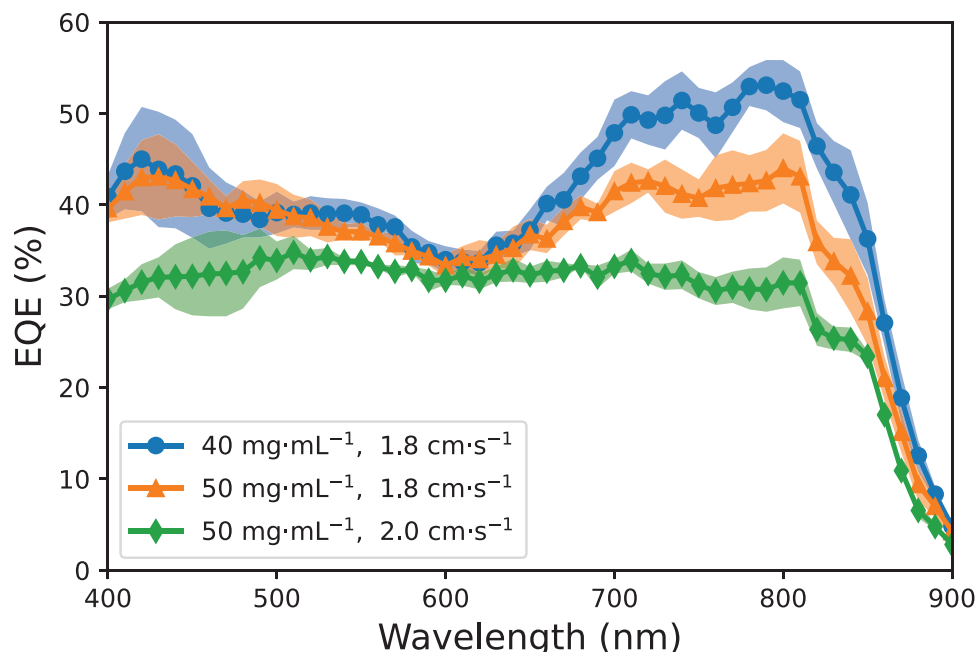


Figure 3. EQE performance of OPDs printed with a combination of coating speeds of 2.0 and 1.8 cm s^{-1} and BHJ solution concentrations of 50 and 40 mg mL^{-1} . All other processing conditions were kept constant. The resulting film thicknesses were 165 nm (green), 140 nm (orange), and 110 nm (blue). EQE was measured at zero applied bias.

spin rate, blade-coated film thickness is directly proportional to the coating speed. A decrease in coating speed results in a decreased film thickness. Similarly, a decrease in solution concentration results in a decrease in solution viscosity (Figure S2, Supporting Information) and thus a decrease in film thickness. Both these parameters enable tunability of device performance through optimization of the film thickness. This is shown in **Figure 3** where the average EQE performance of OPD devices was tuned with adjustments in both coating speed and solution concentration. OPD devices fabricated from 50 mg mL^{-1} BHJ solution and coating speed of 2.0 cm s^{-1} (green) show roughly 30% EQE at a measured film thickness of 165 nm. Decreasing coating speed from 2.0 to 1.8 cm s^{-1} decreased the film thickness to 140 nm, resulting in improved peak EQE to 44% at 800 nm (orange). Using the same coating speed of 1.8 cm s^{-1} with decreased the BHJ solution of 40 mg mL^{-1} , the film thickness decreased to 110 nm and further improved the peak EQE to 53% at 800 nm (blue).

Traditionally in blade coating, one solution is deposited for each printing layer and processing parameters are optimized for that single film. In this work, OPD and OLED solutions are simultaneously printed side-by-side in a single blade coating step. Thus, the blade height and speed, substrate temperature, and annealing conditions are shared processing conditions for both solutions. However, OPD and OLED active layers can require different target film thicknesses to optimize desired device characteristics. OPD BHJ and OLED EML solutions can also have distinct viscosity and wetting properties, adding complexity to developing a single process for dual-device prints. An advantage of SEP is the isolation of two solutions, allowing individual films to be tuned via solution rheological properties such as solution concentration as previously shown. Furthermore,

adjusting individual solution concentrations rather than blade speed enables tuning of one film without affecting the other.

Here, the fabrication process is optimized by chosen figure of merits for each device—spectral responsivity $R(\lambda)$ for OPDs and luminance L_v for OLEDs. The spectral responsivity of a photodiode determines the application space of a photodetector as it quantifies the electrical output of a detector in response to optical input over a range of wavelengths. $R(\lambda)$, in units of A W^{-1} , is defined as the ratio between photocurrent generated I_L and incident optical power P_L as a function of wavelength. The equation is given by:

$$R(\lambda) = \frac{I_L}{P_L} = \eta \frac{q}{hf} = \eta \frac{q\lambda}{hc} \quad (2)$$

where η is the external quantum efficiency of the detector for a given wavelength, q is the elementary charge, f is the frequency of the incident light, h is Planck's constant, and c is the speed of light. Luminance L_v , in units of cd m^{-2} , is a photometric measure of radiance $L(\lambda)$ and is a critical parameter for lighting and display applications. The equation for luminance is given by:

$$L_v = 683 \left[\frac{\text{lm}}{\text{W}} \right] \int_{380}^{770} L(\lambda) \times V(\lambda) d\lambda = 683 \int_{380}^{770} \frac{I_{det} D^2}{R_{det,s} S_0 A_0} \times V(\lambda) d\lambda \quad (3)$$

where $V(\lambda)$ is the visual response of the human eye, I_{det} is the measured photocurrent at the detector, D is the distance between the OLED and the detector, $R_{det,s}$ is the detector responsivity weighted to the measured OLED emission spectrum, S_0 is the OLED emission area, and A_0 is the detector area.

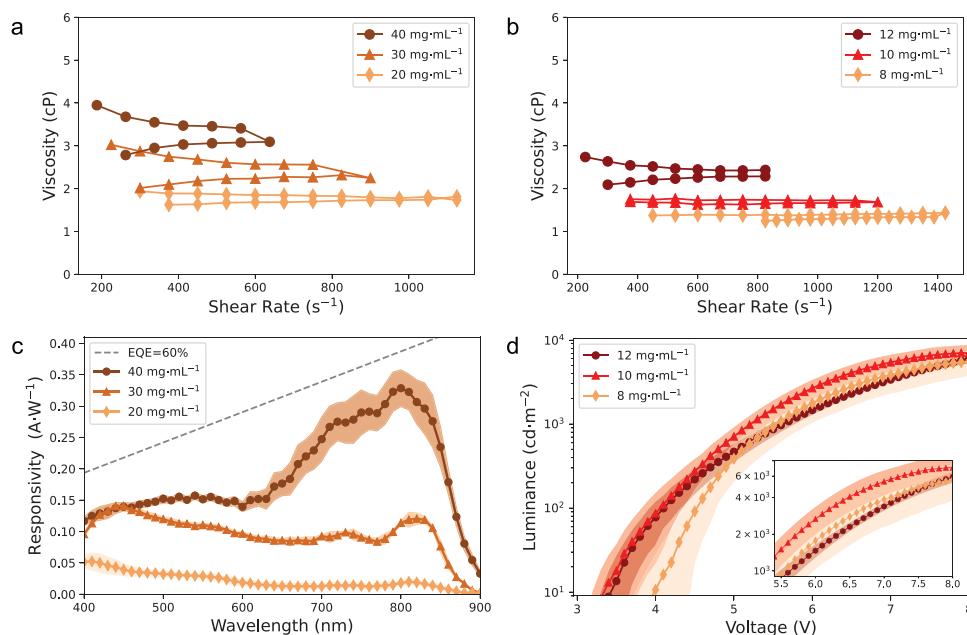


Figure 4. Viscosities of OPD BHJ and OLED EML solutions and average device characteristics of OPD and OLEDs fabricated from those solutions. a) Viscosity versus shear rate of OPD BHJ solutions at concentrations of 40, 30, and 20 mg mL⁻¹. b) Viscosity versus shear rate of OLED EML solutions at concentrations of 12, 10, and 8 mg mL⁻¹. c) Responsivity of printed OPDs with zero applied bias. Spectral responsivity at an EQE of 60% is plotted as a dashed line for reference. d) Luminance of printed OLEDs from 3 to 8 V. The inset plot shows detailed luminance behavior between 5.5 and 8 V.

Figures of merit were characterized for various solution concentrations. For OPDs, BHJ solution concentrations of 40, 30, and 20 mg mL⁻¹ were used resulting in film thicknesses of 110, 75, and 42 nm. For OLEDs, EML solution concentrations of 12, 10, and 8 mg mL⁻¹ were used resulting in film thicknesses of 70, 55, and 45 nm. As the thicknesses of thin organic films stacked atop a flexible substrate can be difficult to measure, film thicknesses were measured from OPD BHJ and OLED EML films printed on plasma-treated glass for simplification. The wettability of organic solutions on plasma-treated glass and on the corresponding printing surface, discussed previously in Figure 2, have negligible differences (Figure S3, Supporting Information). Thus, the films measured on glass are expected to provide film thicknesses suitable for correlating characteristics for devices fabricated from different solution concentrations.

Figure 4 shows viscosity versus shear rate for OPD BHJ and OLED EML solutions and the average performance of OPDs and OLEDs printed with the respective solution concentrations. Viscosities ranged from 1.6 to 3.9 cP for OPD BHJ solutions and 1.2 to 2.7 cP for OLED EML solutions. Each curve in Figures 4c, d represents average and standard deviation characteristics measured from five to ten devices from a single print. Figure 4a shows the spectral response of OPDs under no applied bias measured over a broad wavelength range of 400 to 900 nm. Responsivity values at various wavelengths are summarized in Table 1. The highest overall spectral response was measured from OPDs printed with the 40 mg mL⁻¹ BHJ solution with a peak value of 0.33 A W⁻¹ at 800 nm. Decreasing BHJ solution concentration to 30 and 20 mg mL⁻¹, the responsivity at 800 nm drops to 0.11 and 0.02 A W⁻¹, respectively. OPDs printed with BHJ solution concentrations lower than 40 mg mL⁻¹ exhibit poor absorption, shown in Figure S4 (Supporting Information),

leading to poor efficiencies. This suggests the ideal BHJ solution concentration for the printing process and material used is around 40 mg mL⁻¹. Figure 4b shows luminance versus voltage performance for three printed OLEDs. Devices from all three solution concentrations exhibit clean diode behavior and average luminance greater than 5000 cd m⁻² at 8V. The electroluminescence spectra measured from OLEDs printed with the three solution concentrations exhibit no noticeable shifts, with consistent peaks at 612 nm, shown in Figure S5 (Supporting Information). The highest OLED luminance achieved among the three EML solution concentrations was around 7000 cd m⁻² from 10 mg mL⁻¹, followed by 12 and 8 mg mL⁻¹. Furthermore, the lowest turn-on voltage and lowest operating voltage (voltage required to achieve a luminance of 1000 cd m⁻²) was achieved with 10 mg mL⁻¹ EML solution. The thinnest EML film from the 8 mg mL⁻¹ solution had the highest turn-on voltage as well as the largest variability in luminance values. This is attributed to more pronounced exciton quenching for thinner emissive films in which recombination occurs closer to the electrode.^[23–25] Overall, the highest luminance and lowest turn-on voltage were achieved with 10 mg mL⁻¹, summarized in Table 2.

Table 1. Comparison of responsivities at wavelengths of 500, 600, 700, and 800 nm for printed OPDs with BHJ solution concentrations of 40, 30, and 20 mg mL⁻¹.

R [A W ⁻¹]	$\lambda = 500$ nm	$\lambda = 600$ nm	$\lambda = 700$ nm	$\lambda = 800$ nm
40 mg mL ⁻¹	0.15	0.14	0.25	0.33
30 mg mL ⁻¹	0.12	0.097	0.092	0.11
20 mg mL ⁻¹	0.032	0.019	0.013	0.018

Table 2. Comparison of turn-on voltage, 1000 cd m⁻² operating voltage, and luminance at 8 V of printed OLEDs with EML solution concentrations of 12, 10, and 8 mg mL⁻¹.

	V _{turn-on} [V]	V _{L=1000 cd m⁻²} [V]	L _{@8V} [cd m ⁻²]
12 mg mL ⁻¹	3.5	5.7	5900
10 mg mL ⁻¹	3.4	5.3	7000
8 mg mL ⁻¹	4	5.6	5600

2.3. OPD Characterization

Figure 5 shows device characteristics of an OPD printed using the optimized BHJ solution concentration of 40 mg mL⁻¹. Current density–voltage (*J*-*V*), external quantum efficiency (EQE), linear dynamic range (LDR), and frequency response of a printed OPD is shown. Figure 5a shows the semilog plot of *J*-*V* characteristics. Photodetectors operate under reverse bias, or photoconductive mode, in which low dark current is desired for detection of low-intensity signals. A low dark current of 22 nA cm⁻² at a bias of -1 V is observed. Under 7 μW cm⁻² illuminations at 532 nm, the current density reaches 1.5 μA cm⁻² at -1 V. OPD EQE between 30% and 40% is observed across the visible spectrum and increases to 40–50% in the NIR spectrum. The EQE profile peaks at 750 and 800 nm with efficiencies of 54% and 56%, respectively. The range of intensities in which the detector's electrical response is linear to incident illumination, linear dynamic range (LDR), is expressed by:

$$\text{LDR} = 20 \times \log \frac{i_{\text{lin, max}}}{i_{\text{lin, min}}} \quad (4)$$

where $i_{\text{lin, max}}$ and $i_{\text{lin, min}}$ is the maximum and minimum photocurrent in the linear response region of the photodetector. Printed OPDs show good linear response of 88 dB in Figure 5c, demonstrating that the device can operate under illumination intensities ranging over four orders of magnitude. Frequency response measures the detection speed of OPDs. The 3 dB bandwidth, or cut-off frequency $f_{3 \text{ dB}}$, is defined as the frequency at which output power of the detector is attenuated by 50% in response to modulating light signals. The equation is given by:

$$-3 \text{ dB} = 20 \times \log \frac{i(f_{3 \text{ dB}})}{i_0} \quad (5)$$

where $i(f_{3 \text{ dB}})$ and i_0 are the photocurrents in response to illumination at the cut-off frequency and steady-state, respectively. The measured cutoff frequency was 300 kHz, as shown in Figure 5d.

2.4. OLED Characterization

Figure 6 shows device characteristics of an OLED simultaneously printed using the optimal EML solution concentration of 10 mg mL⁻¹. The current density–voltage (*J*-*V*), luminance, EQE, luminous efficacy, and electroluminescence spectrum are shown. The OLED exhibits clean diode behavior with a turn-on voltage of 3.1 V at a current density of 1.9 mA cm⁻². A luminance of 7980 cd m⁻² is measured at 8 V. A luminance of 1000 cd m⁻² can be achieved at an operating voltage of 4.8 V. Luminous efficacy η_{lum} is defined as the ratio of luminous flux

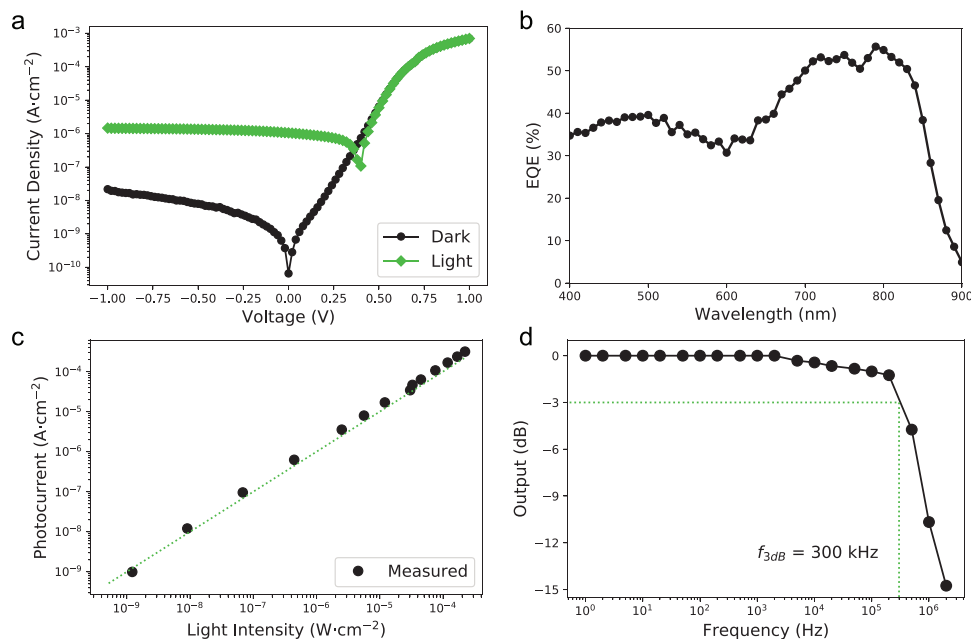


Figure 5. Device characteristics of an OPD simultaneously printed using a 40 mg mL⁻¹ BHJ solution concentration. a) Current density versus voltage (*J*-*V*) measured under dark and illumination, b) external quantum efficiency (EQE) in the wavelength range of 400–900 nm, c) linear dynamic range (LDR) and d) frequency response. Light current, LDR, and frequency response were measured with a 532 nm LED at 7 μW cm⁻² illuminations. No bias was applied to the OPD during EQE, LDR, and cut-off frequency measurements.

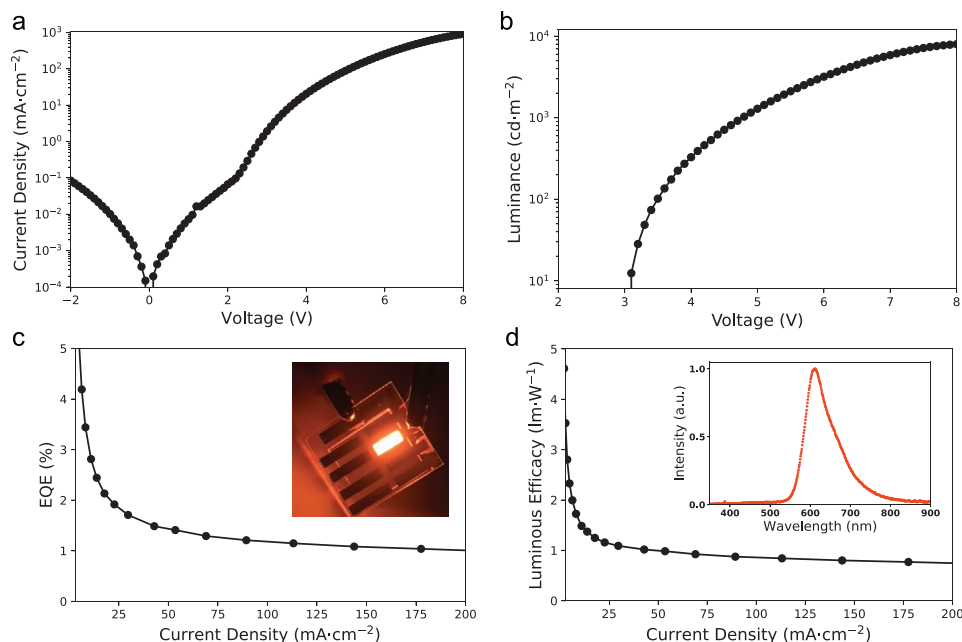


Figure 6. Device characteristics of an OLED simultaneously printed using a 10 mg mL⁻¹ EML solution concentration. a) Current density versus voltage (*J*-*V*), b) luminance versus voltage (*L*-*V*), c) EQE versus current density with inset image of OLED operated at 6 V, and d) luminous efficacy versus current density with inset plot of the OLED electroluminescence spectrum.

Φ_v , in lumens, emitted to the electrical input power *P*, in Watts. It can be expressed as:

$$\eta_{lum} = \frac{\Phi_v}{P} \quad (6)$$

Printed OLED EQE and luminous efficacy steady to roughly 1% and 1 lm W⁻¹, respectively, for current densities above 100 mA cm⁻². At a luminance of 1000 cd m⁻² the EQE and luminous efficacy is 1.2% and 0.9 lm W⁻¹. The inset of Figure 6c shows an image of the printed OLED operated at 6 V. The inset of Figure 6d shows the electroluminescence spectra of the printed OLED with a peak at 612 nm.

3. Conclusion

A method for simultaneous blade coating of two different films is demonstrated. SEP isolates printing regions, enabling the deposition of two functionally opposing materials side-by-side on a single flexible substrate. Here, the OPD BHJ and OLED EML film thicknesses were tuned via adjustments in solution concentrations. This enables the use of a single process for the fabrication of two devices without compromising device performances. The resulting dual device structure eliminates the need for laminating OPD and OLED substrates, retaining the mechanical flexibility of lightweight optoelectronic systems while allowing for simplified integration to electronic circuitry. This method demonstrates an important step toward roll-to-roll printing where integration of devices with different functionalities is needed.

4. Experimental Section

Surface Energy Patterning: PEN substrates mounted on glass carrier substrates were patterned with two 10 mm wide ITO strips with an 11 mm separation and provided by Cambridge Display Technologies (CDT). The PEN/ITO substrates were placed overnight in a vacuum oven at 80 °C then heated on a hotplate at 180 °C for 30 min in the atmosphere. Following activation with low energy plasma, the substrate was treated with (heptadecafluoro-1,1,2,2-tetrahydrodecyl)trichlorosilane (Gelest SIH5841.0) for 20 min to create a hydrophobic surface. Polyimide tape was applied to specific regions of the substrate, leaving 2 cm width bands of the substrate exposed to low energy plasma, resulting in two hydrophilic printing regions surrounded by hydrophobic boundaries.

Device Fabrication: All blade coating steps were completed on hotplates with a doctor blade (Zehntner ZUA 2000.60) and linear actuators (Servo City). After removing the polyimide tape, PEDOT:PSS (Clevios AI4083, Heraeus) was blade-coated with a blade height, coating speed, and hotplate temperature of 50 μm, 1.8 cm s⁻¹, and 90 °C, respectively. The films were annealed at 130 °C for 10 min. The substrate was then transferred to a nitrogen inert glovebox to print the active layers. Semiconducting organic materials used for OPD BHJ, OLED EBL, and EML were provided by CDT. The OLED electron blocking and emissive materials provided were dissolved in *o*-Xylene. An equivalent material combination that can be used as the emissive layer is a mixture of poly((9,9-dioctylfluorene-2,7-diyl)-alt-(2,1,3-benzothiadiazole-4,8-diyl)) (F8BT), poly(9,9-dioctylfluorene-co-N-(4-butylphenyl)-diphenylamine) (TFB), and poly((9,9-dioctylfluorene-2,7-diyl)-alt-(4,7bis(3-hexylthiophene-5-yl)-2,1,3-benzothiadiazole)-2',2'-diyl)^[8] with TFB as the electron blocking layer. The OPD absorbing materials provided by CDT have dissolved in 95:5 1,2,4-trimethylbenzene:benzyl benzoate. A similar material combination that can be used is 2,2'-((2Z,2'Z)-(((4,4,9,9-tetrakis(4-hexylphenyl)-4,9-dihydro-sindaceno[1,2-b:5,6-b']dithiophene-2,7-diyl) bis(4-((2-ethylhexyl)oxy)thiophene-5,2-diyl)) bis(methanylylidene)bis(5,6-difluoro-3-oxo-2,3-dihydro-1H-indene-2,1-diylidene))dimalononitrile (IEICO-4F) and poly([2,6'-4,8-di(5-ethylhexylthienyl)benzo[1,2-b:3,3-b']dithiophene]3-fluoro-2[(2-ethylhexyl)carbonyl]thieno [3,4-b]thiophenediyl) (PTB7-Th).^[26]

The electron blocking interlayer is printed for the OLED stack at a blade height, blade speed, and hotplate temperature of 50 μm , 1.8 cm s^{-1} , and 65 $^{\circ}\text{C}$ followed by annealing at 180 $^{\circ}\text{C}$ for 1 h. After annealing, the hotplate is cooled and reset to 65 $^{\circ}\text{C}$ for printing the OPD BHJ and OLED EML at a blade height and speed of 200 μm , 1.8 cm s^{-1} . The films were annealed at 140 $^{\circ}\text{C}$ for 30 min. The sample was attached to a shadow mask and transferred to a thermal evaporator for evaporation of the cathode. For OLED devices, 10 nm of calcium (99.5%, STREM CHEMICALS) and 100 nm of aluminum (99.999%, ACI ALLOYS INC) were evaporated. For OPD devices, 100 nm of aluminum was evaporated. OLED devices were encapsulated with UV curable epoxy (DELO Photobond LP4224) and PEN films.

Film Thickness Characterization: OPD BHJ and OLED EML films were printed on plasma-treated glass substrates and film thicknesses were measured with a Keyence VK-X1000 Laser Scanning Confocal Microscope.

Solution Viscosity: OPD BHJ and OLED EML solutions were prepared at various concentrations and measured with a Brookfield Model DV-III Programmable Rheometer attached with a CP-40 cone spindle.

Device Performance Characterization: Keithley 2601, Keithley 2400, and silicon photodiode setup were used to measure J - V - L of the OLED devices. The emission spectra and fluxes were measured with a spectrometer (SP-75, Orboptronix), integrating sphere and Keithley 2601. The OPD device J - V , frequency response, and LDR were measured using an Agilent B1500a semiconductor parameter analyzer and LED setup. OPD EQEs were measured using PV Measurements QEXL system.

Statistical Analysis: Plots in Figures 3 and 4 show the average and one standard deviation of performances from five to ten devices measured from a single print condition.

Supporting Information

Supporting Information is available from the Wiley Online Library or from the author.

Acknowledgements

J.J., J.Z., and J.T. contributed equally to this work. This work was partially supported by the National Science Foundation Graduate Research Fellowship under Grant No. DGE 1752814 and NIH U01EB029427. The authors thank Cambridge Display Technology (CDT) for supplying organic materials and flexible substrates.

Conflict of Interest

The authors declare no conflict of interest.

Data Availability Statement

The data that support the findings of this study are available from the corresponding author upon reasonable request.

Keywords

blade coating, flexible, organic light-emitting diodes, organic photodiodes, printed

Received: December 3, 2021

Revised: February 11, 2022

Published online:

- [1] H. R. Lim, H. S. Kim, R. Qazi, Y. T. Kwon, J. W. Jeong, W. H. Yeo, *Adv. Mater.* **2020**, 32, 1.
- [2] Y. Ma, Y. Zhang, S. Cai, Z. Han, X. Liu, F. Wang, Y. Cao, Z. Wang, H. Li, Y. Chen, X. Feng, *Adv. Mater.* **2020**, 32, 1.
- [3] D. Zhang, T. Huang, L. Duan, *Adv. Mater.* **2020**, 32, 1.
- [4] J. A. Rogers, T. Someya, Y. Huang, *Science (80-)*. **2010**, 327, 1603.
- [5] M. Kuik, G. J. A. H. Wetzelaer, H. T. Nicolai, N. I. Craciun, D. M. De Leeuw, P. W. M. Blom, *Adv. Mater.* **2014**, 26, 512.
- [6] S. J. Benight, C. Wang, J. B. H. Tok, Z. Bao, *Prog. Polym. Sci.* **2013**, 38, 1961.
- [7] T. Sekitani, T. Someya, *Adv. Mater.* **2010**, 22, 2228.
- [8] C. M. Lochner, Y. Khan, A. Pierre, A. C. Arias, *Nat. Commun.* **2014**, 5, 5745.
- [9] H. Jinno, T. Yokota, M. Koizumi, W. Yukita, M. Saito, I. Osaka, K. Fukuda, T. Someya, *Nat. Commun.* **2021**, 12, 4.
- [10] Y. Khan, D. Han, A. Pierre, J. Ting, X. Wang, C. M. Lochner, G. Bovo, N. Yaacobi-Gross, C. Newsome, R. Wilson, A. C. Arias, *Proc. Natl. Acad. Sci. USA* **2018**, 115, E11015.
- [11] A. Pierre, M. Sadeghi, M. M. Payne, A. Facchetti, J. E. Anthony, A. C. Arias, *Adv. Mater.* **2014**, 26, 5722.
- [12] M. Sadeghi, P. Delparastan, A. Pierre, A. C. Arias, *Adv. Electron. Mater.* **2020**, 6, 1901207.
- [13] D. Han, Y. Khan, J. Ting, S. M. King, N. Yaacobi-Gross, M. J. Humphries, C. J. Newsome, A. C. Arias, *Adv. Mater.* **2017**, 29, 1606206.
- [14] D. Han, Y. Khan, K. Gopalan, A. Pierre, A. C. Arias, *Adv. Funct. Mater.* **2018**, 28.
- [15] J. Zhu, D. Han, X. Wu, J. Ting, S. Du, A. C. Arias, *ACS Appl. Mater. Interfaces* **2020**, 12, 31687.
- [16] A. Pierre, I. Deckman, P. B. Lechêne, A. C. Arias, *Adv. Mater.* **2015**, 27, 6411.
- [17] I. Deckman, P. B. Lechêne, A. Pierre, A. C. Arias, *Org. Electron.* **2018**, 56, 139.
- [18] A. E. Ostfeld, A. M. Gaikwad, Y. Khan, A. C. Arias, *Sci. Rep.* **2016**, 6.
- [19] R. L. Davis, S. Jayaraman, P. M. Chaikin, R. A. Register, *Langmuir* **2014**, 30, 5637.
- [20] C. M. Stafford, K. E. Roskov, T. H. Epps, M. J. Fasolka, *Rev. Sci. Instrum.* **2006**, 77, 023908.
- [21] A. C. Grimsdale, K. L. Chan, R. E. Martin, P. G. Jokisz, A. B. Holmes, *Chem. Rev.* **2009**, 109, 897.
- [22] Y. Huang, E. J. Kramer, A. J. Heeger, G. C. Bazan, *Chem. Rev.* **2014**, 114, 7006.
- [23] S. Höfle, T. Lutz, A. Egel, F. Nickel, S. W. Kettlitz, G. Gomard, U. Lemmer, A. Colmann, *ACS Photonics* **2014**, 1, 968.
- [24] C. Schmitz, M. Thelakkat, H. W. Schmidt, *Adv. Mater.* **1999**, 11, 821.
- [25] A. L. Burin, M. A. Ratner, *J. Phys. Chem. A* **2000**, 104, 4704.
- [26] X. Song, N. Gasparini, L. Ye, H. Yao, J. Hou, H. Ade, D. Baran, *ACS Energy Lett.* **2018**, 3, 669.